An analysis of a swimmer's passive wave resistance using experimental data and CFD simulations

Banks J., James M., Hudson D., Taunton D., Turnock S.
Fluid-Structure Interactions Research Group; University of Southampton, SO17 1BJ, Southampton, UK

1 Introduction

The passive resistance of a swimmer on the free surface has previously been researched experimentally. The contribution of wave resistance to total drag for a swimmer with a velocity around 2.0 m.s^{-1} was found to vary from 5% for Vorontsov and Rumyantsev (2000), to 21 % for Toussaint et al. (2002) and up to 60% according to Vennell et al. (2006). The exact resistance breakdown of a swimmer remains unknown due to difficulties in the direct measurement of wave resistance. As noted by Sato and Hino (2010), this lack of experimental data makes it difficult to validate numerical simulations of swimmers on the free surface.

This study is therefore aimed at presenting direct measurements of a swimmer's total drag and wave resistance, along with the longitudinal wave cuts which may be used to validate numerical simulations. In this paper, experimental data of a swimmer's resistance are presented at two different velocities (case 1 = 1.7 m.s^{-1} and case 2 = 2.1 m.s^{-1}). Total drag was measured using force block dynamometers mounted on a custom-built tow rig (Webb et al., 2011). Moreover, a longitudinal wave cut method was used to directly evaluate wave resistance (Eggers, 1955).

The two conditions tested were simulated using the open-source Computational Fluid Dynamics (CFD) code OpenFOAM (OpenFOAM® (2013)). The body geometry is a generic human form, morphed into the correct attitude and depth using the above- and under-water video footage recorded during the experiment. 3D Unsteady Reynolds-Averaged Navier-Stokes (URANS) simulations were performed using the Volume of Fluid (VOF) method to solve the air-water interface. A similar numerical technique was used by Banks (2013a) to assess the passive resistance of a swimmer. Two cases were simulated and the error in total drag compared to the experimental data was found to be 1 % and 22 % respectively. In this paper, the resistance components over a swimmer's typical range of speeds are investigated and compared with the experimental data.

2 Methods

2.1 Experimental set-up and analysis

A male swimmer (height = 1.78 m, weight = 66 kg) was towed passively along a 25-m pool, with their arms by their side, with a tow belt fixed around his waist. Two speeds were chosen across the range of typical swimming speeds: 1.7 m.s^{-1} (case 1) and 2.1 m.s^{-1} (case 2). Both total resistance and wave resistance were measured. The experimental set-up is presented in Figure 1.

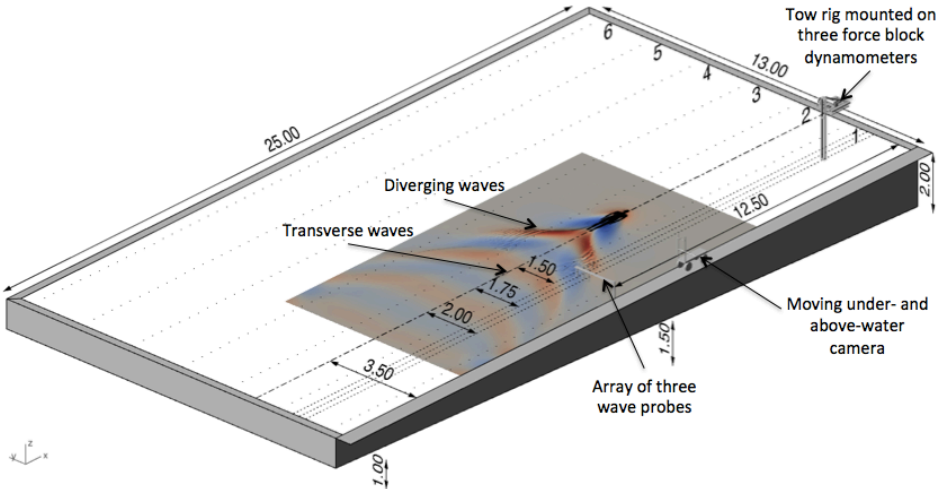

Figure 1 – Schematic of the University of Southampton Jubilee swimming pool with infinity edges

The total resistance was obtained by averaging data from the force-block dynamometers mounted on a custom-built tow winch. The instrumented tow system allows the swimmer to be pulled along the pool at a constant speed whilst the tow force is measured using three force blocks (Webb et al., 2011). The magnitude of the measured force is calibrated at the beginning of each session by applying a known force to the system. A moving camera allows a synchronised video feed to be acquired at the same time.

The wave pattern resistance was obtained using a longitudinal wave cut method originally defined by Eggers (1955), developed by Insel (1990) and refined by . This method assumes that a slender body is moving in an inviscid, incompressible and homogeneous fluid and that the resulting flow is steady and irrotational. Furthermore, the wave height should be significantly smaller than the wave length. A tripod was set halfway along the pool (x = 12.5 m) with an array of three wave probes located at distances y = 1.50, 1.75 and 2.00 m away from the track of the swimmer. These wave probes are made of two parallel stainless steel wires, 12 mm apart. The conductivity between air and water is significant enough that a change in voltage output can be measured as the water surface deforms. The probes were calibrated by acquiring the voltage output at two known immersion depths +/- 0.1 m as they have known linearity response.

During a run, three longitudinal wave cuts were recorded at a sample rate of 250 Hz. A numerical wave profile was fitted through each experimental wave cut and the matrix method developed by Insel (1990) was used to determine the Eggers coefficients ξ_n and η_n, leading to the full wave system definition.

$$\zeta = \sum_{n=0}^{M}[\xi_n \cos(x\gamma_n cos\theta_n) + \eta_n \sin(x\gamma_n cos\theta_n)] * \cos\frac{2\pi n y}{b}$$

where, $\gamma_n sin\theta_n = \frac{2\pi n}{b}$, θ_n is the wave angle, b is the width of the domain and M is the number of harmonics.

Theoretically, only one longitudinal wave cut is necessary to evaluate the wave elevation, ζ, but in case the term $\cos\frac{2\pi n y}{b} \to 0$ for some harmonics, longitudinal wave cuts from the two wave probes closest to the swimmer were used for the analysis.

Once the Eggers coefficients are found, the wave resistance can be calculated as follows:

$$R_w = \frac{1}{4}\rho g b\left\{(\xi_0^2 + \eta_0^2) + \sum_{n=1}^{M}(\xi_n^2 + \eta_n^2)\left(1 - \frac{1}{2}\cos^2\theta_n\right)\right\}$$

2.2 Computational Fluid Dynamics

2.2.1 Swimmer geometry

A generic body scan of a human with their arms by their sides was used as a basis athlete geometry. The basis athlete geometry was modified with an in-house meshing tool called Adaptflexi (Turnock, 2004) so as to match the different case conditions. This has the capability to take a .STL geometry and deform it in a number of different ways. Firstly, variable scale factors are applied along the body to match a specific athlete's body shape. Secondly, joint rotations are performed to match the athlete's attitude and posture from the video footages acquired during the experiment (Figure 2).

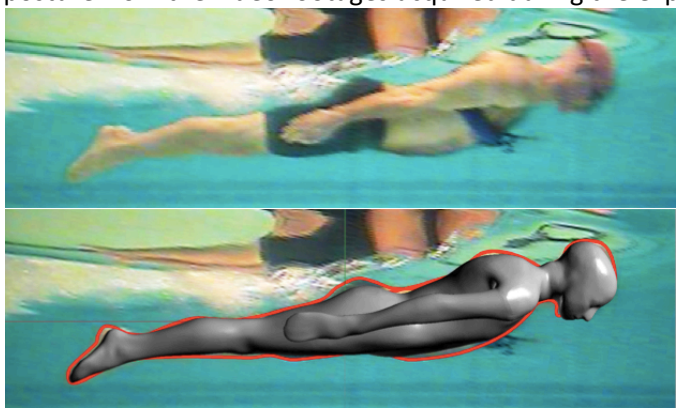

Figure 2 – Swimmer's position from the under-water view used to modify a generic scanned body

2.2.2 Meshing technique

An unstructured hexahedral mesh around the swimmer was created using the snappyHexMesh utility within the open source CFD package OpenFOAM-2.2.0 (OpenFOAM®, 2013). First, a coarse block mesh with dimensions 14 x 7.5 x 2 [m^3] was created with cells of 0.2 m in each direction. Regions were defined with up to six levels of isotropic refinement (recursively having in all three local cell dimensions six times), gradually increasing the mesh density near the body, whilst maintaining a cell aspect ratio of approximately one. Unidirectional refinement was applied perpendicular to the free surface to provide good wave pattern resolution, whilst minimising mesh size. Boundary layer elements were grown out from the body surface mesh to provide a y^+ of 1. This places approximately 10 cells within an estimated y^+ of 40 allowing the viscous boundary layer to be captured (WS Atkins Consultants, 2003). The developed mesh structure contains approximately eight million elements and is shown in side elevation and plan view (Figure 3).

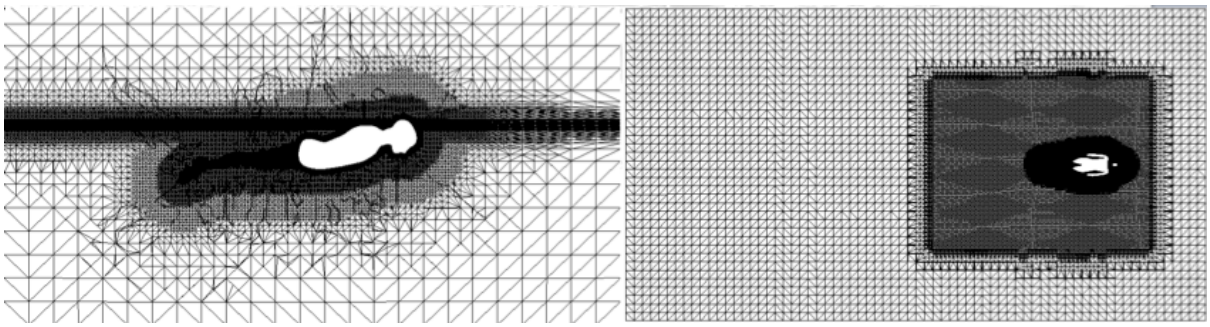

Figure 3 - Mesh at plan y = 0 m (left) and plan z = -0.2 m (right)

2.2.3 Numerical approach with the inclusion of a free-surface

The fluid properties around the swimmer were solved with the Unsteady incompressible Reynolds-Averaged Navier-Stokes (URANS) equations using a second order PISO finite volume method. The fluid temperature was set to 25°C with a density of 997 kg.m^{-3} and a kinematic viscosity of 0.89 x 10^{-6} $m^2.s^{-1}$. The k-ω SST turbulence model was applied since it provides a reasonable representation of a boundary layer under adverse pressure gradients, separation and recirculation. A Volume of Fluid (VOF) approach was used for the free surface with the volume fraction transport equation defined as:

$$\frac{\partial \varphi}{\partial t} + \frac{\partial (\varphi U_j)}{\partial x_j} = 0$$

where ϕ is the volume fraction calculated as the volume ratio of water to air in a given cell (Peric, M., & Ferziger, 2002). The fluid density, ρ, and viscosity, μ, can then be respectively calculated as:

$$\rho = \rho_{air}(1-\varphi) + \rho_{water}\varphi \quad \text{and} \quad \mu = \mu_{air}(1-\varphi) + \mu_{water}\varphi$$

The detailed numerical settings used to perform the multi-phase simulations discussed in this paper can be found for similar simulations in Banks (2013b). These simulations were computed in parallel runs on the high performance computing facility available at the University of Southampton Iridis 4 (10x16 core nodes each with 4GB RAM/core). At the lowest speed, seven hours were required to simulate one second of real time and the simulations were run for 25 seconds in order to capture three flows through the domain.

3 Results

The wave fields observed around the swimmer during the experimental tests and as obtained from CFD are presented in Figure 4 and 5. At the higher speed (case 2 – V = 2.1 m.s^{-1}), more energy is transferred to the wave system resulting in a larger-amplitude wave pattern. Consequently, a higher wave resistance is obtained in this case as indicated in Table 1 (on average 26 % increase between case 1 and case 2).

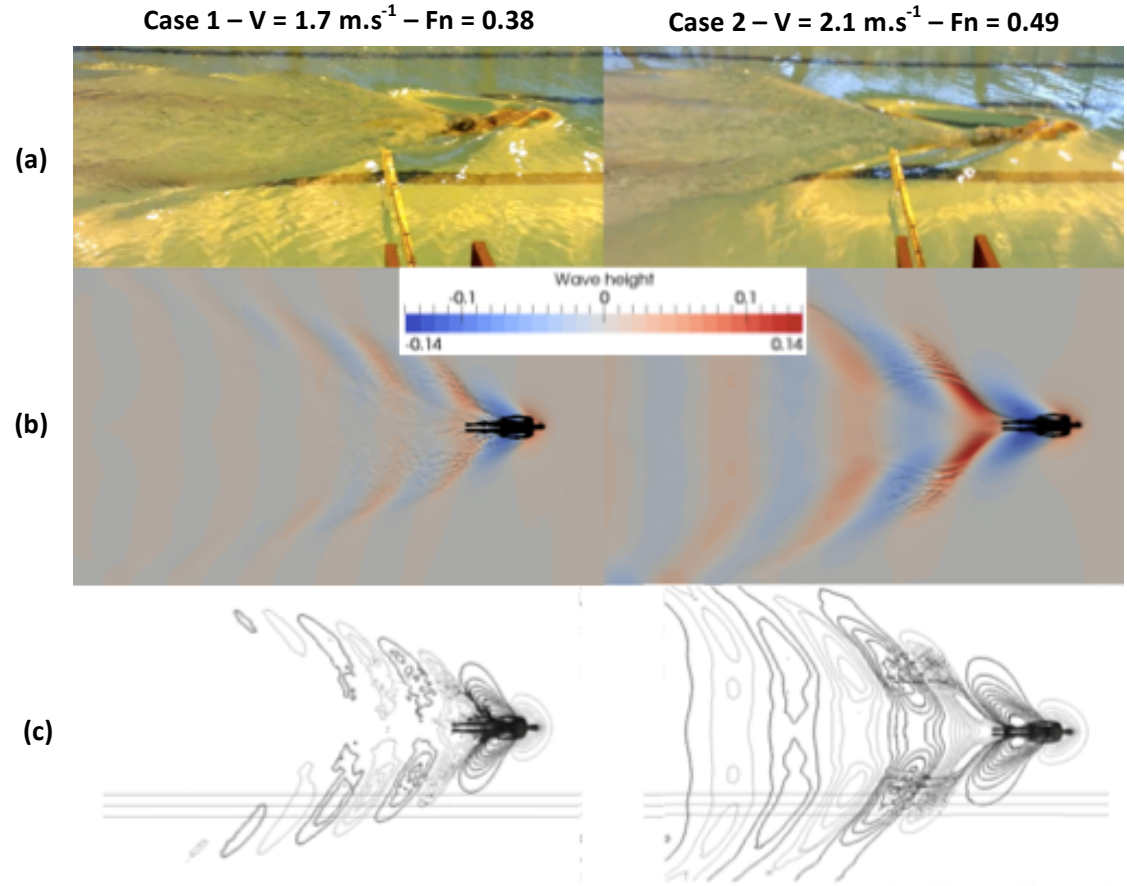

Figure 4 – A comparison of the wave pattern observed around the swimmer during the experimental tests (a) with the numerical solution (b, c) of the free surface. Free surface deformation displayed with contours ±0.01m (bold contours are wave trough) and longitudinal wave cuts positioned at y = 1.50, 1.75 and 2.00 m away from the swimmer (c).

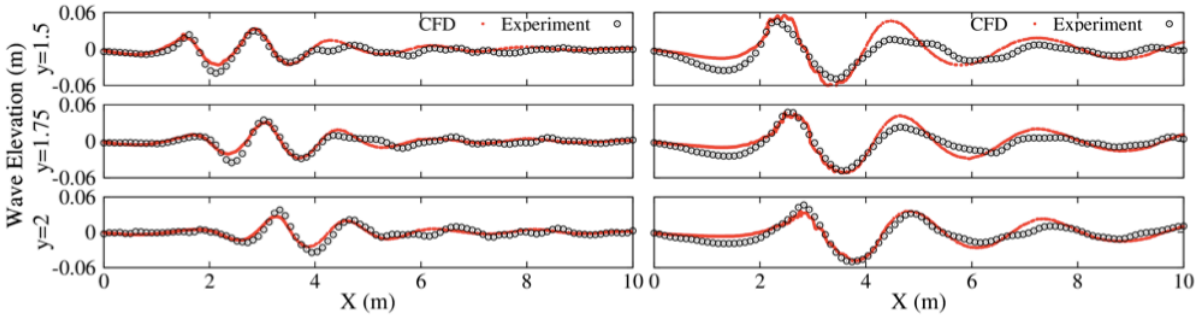

Figure 5 – A comparison of the experimental and numerical longitudinal wave cuts at different offset distances (y) from the centerline (Case 1 (left) and Case 2 (right))

As presented in Tables 1 and 2, the total swimmer's passive resistance breaks down to the sum of the skin friction and pressure force. This last term can be further expressed in terms of the viscous pressure form and the wave drag. The CFD skin friction and total pressure force were obtained by taking the average values of two steady flows through.

The experimental data evaluated using the methodology described in 2.1 confirms a higher wave resistance at the highest speed; however the percentage of drag due to wave resistance increases as the speed decreases. Averaging the data over three repeat runs, wave resistance represents 13.7 % of the total drag at 1.7 $m.s^{-1}$, whereas at the higher average speed tested of 2.1 $m.s^{-1}$, wave resistance accounts for only 11.5% of the total drag.

Table 1 – Case 1 (Speed = 1.7 m.s^{-1}) – ***Measured values***

Resistance [N]		**ITTC'57 coeff.** (ITTC, 2002)	**Experiment**	**CFD**		
				Force [N]	**% R_T**	**Coeff. [-]**
Skin friction		3.61E-03		***10.43***	10.75%	3.78E-03
Pressure	P-viscous (form)					
	P-wave		***18.07, 14.68, -***			
	P-total (P-v + P-w)			***86.58***	89.25%	31.4E-03
Total			***120.1, 119.7, 118.3***	97.01	100.00%	35.1E-03

Table 2 – Case 2 (Speed = 2.1 m.s^{-1}) – ***Measured values***

Resistance [N]		**ITTC'57 coeff.** (ITTC, 2002)	**Experiment**	**CFD**		
				Force [N]	**% R_T**	**Coeff. [-]**
Skin friction		3.45E-03		***16.86***	11.25%	3.71E-03
Pressure	P-viscous (form)					
	P-wave		***17.21, 24.90, 23.41***			
	P-total (P-v + P-w)			***132.98***	88.75%	29.3E-03
Total			***183.4, 195.3, 193.1***	149.84	100.00%	33.0E-03

4 Discussion

The numerical simulation effectively captured the wave system developed by the swimmer in a comparable manner to the experiment, as seen in Figure 5. Overall, there is a better agreement with the wave probe located closer to the swimmer and for the near-wake.

The discrepancy between the numerically simulated free surface elevation and the measured longitudinal wave cuts comes from several factors. In a pool, there is only a partial wall reflection, whereas in the CFD a solid boundary is simulated. Furthermore, during the experiment, the free surface was never perfectly calm, despite time being allowed for the pool water surface to settle. This may have caused small wave interactions resulting in different wave resistances over the experimental set of runs. Numerical diffusion may also cause the simulated wave pattern to dissipate further away from the swimmer.

Another major unknown is the variability in the swimmer's position during a run. Indeed, a swimmer cannot physically adopt a steady position whilst being towed. His vertical position is governed by balancing the buoyancy, weight and hydrodynamic forces. His attitude in the water is dictated by the moments generated by these forces. For instance, the distance between the centres of buoyancy and gravity generates a moment which tends to pitch the feet down. Increase in a swimmer's angle of attack leads to a larger frontal area, resulting in a higher drag as identified in Tables 1 and 2. As the fluid forces and moments acting on a swimmer's body are unsteady, the athlete naturally controls his position in the water with small movements of his body, which are not captured in the simulations.

All these factors are currently not directly quantifiable but are known to have a significant impact on the various resistance components. It is noted that these variations can be seen in the recorded line tension and are averaged for each of the three repeat runs (the coefficient of variation is 6 %). The ITTC (1967) resistance committee reported a study from Maruo and Ishii, which considered different underwater hull forms in the near free surface to reduce wave resistance. These results emphasise the substantial impact of a body volume and position near the free surface on the wave resistance. The described sources of error can explain: the discrepancy between the numerical simulations and the experimental data, and the differences between repeated experimental runs.

5 Conclusions

To the authors' knowledge, this paper presented the first direct measurements of the passive wave resistance of a swimmer with the use of a longitudinal wave cut and matrix analysis used in naval architecture. On average, wave resistance represents 13.7 % of the total drag at 1.7 $m.s^{-1}$ and 11.5% of the total drag at 2.1 $m.s^{-1}$. It is important to note that these values are specific to the swimmer body geometry and position adopted during the experimental runs presented. More repeat runs of the same athlete and other athletes with different body geometries would be necessary to establish a relationship between body geometry and position with respect to the free surface and wave resistance.

The numerical simulations effectively captured the fundamental flow features of the wave system generated by the swimmer. However, a comprehensive validation of CFD simulations remains difficult because of human variability and discrepancies in the geometry. The uncertainties associated with towing a human swimmer would be alleviated through the use of a captive mannequin in a towing tank to ensure repeatable conditions, which can be more easily compared with the numerical simulations.

Acknowledgments

The authors would like to acknowledge the University of Southampton for the use of the supercomputer Iridis 4 and the PhD sponsors: EPSRC, English Institute of Sport, British Swimming and Speedo.

References

Banks, J. (2013a), Modelling the propelled resistance of a freestyle swimmer using Computational Fluid Dynamics, PhD Thesis, University of Southampton.

Banks, J. (2014), Kayak blade-hull interactions: a body-force approach for self-propelled simulations, Proceedings of the Institution of Mechanical Engineers, Part P, Journal of Sports Engineering and Technology, 228 (1), 49-60.

Eggers, K. (1955), Resistance components of two-body ships, Jahrbuch der Schiff- bautechnischen Gesellschaft, 49.

Insel, M. (1990), An investigation into the resistance components of high speed displacement catamarans, PhD thesis, University of Southampton.

ITTC (1967), Report of resistance committee, 66-79.

ITTC (2002), Report of the specialist committee on procedures for resistance, propulsion and propeller open water tests, Recommended procedure for open water tests, No. 7.5-02-03-02.1.

Larsson, L., Stern, F., & Bertram, V. (2003), Benchmarking of Computational Fluid Dynamics for Ship Flows: The Gothenburg 2000 Workshop.

Molland, A. F., Turnock, S. R. and Hudson, D. A. (2011), Ship resistance and propulsion: practical estimation of propulsive power, 131-135.

OpenFOAM® (2013), *OpenFOAM – The Open Source CFD Toolbox- User Gide, Version 2.2.0.*

Peric, M., & Ferziger, J. H. (2002), *Computational Methods for Fluid Dynamics*, Berlin: Springer.

Toussaint, H.M., van Stralen, M. and Stevens, E. (2002), Wave drag in front crawl swimming, Proceedings of the XXth International Symposium on Biomechanics in Sports, Spain, 279-282.

Vennell, R., Pease, D. and Wilson, B. (2006), Wave drag on human swimmers, Journal of Biomechanics, 39, 664-671.

Vorontsov, A.R. and Rumyantsev, V.A. (2000), Resistive forces in swimming. In: Zatsiorsky, V. (Ed.), Biomechanics in Sports: Performance Enhancement and Injury Prevention. Vol. IX Encyclopaedia of Sports Medicine. Blackwell, IOC Medical Commission (Chapter 9).

Taunton, D.J. (2013) In-house slender body theory code (waveSis), University of Southampton.

Turnock, S. R. (2004), Parametric definition of complex multi-appended bodies for marine and aerospace application: a user-guide to Adaptflexi, University of Southampton.

Webb, A.P., Banks, J., Phillips, C.W.G., Hudson, D.A., Taunton, D.J., Turnock, S.R. (2011), Prediction of passive and active drag in swimming, Procedia Engineering, 13, 133-140.

WS Atkins Consultants (2003), Best Practice Guidelines for Marine Applications of Computational Fluid Dynamics.